TECHNICAL ARTICLE

Comparison of Wear Performance of Low Temperature Nitrided and Carburized 316L Stainless Steel under Dry Sliding and Corrosive-Wear Conditions

Y. Sun and R. Bailey

316L austenitic stainless steel was plasma nitrided and carburized at low temperatures to produce precipitation-free nitrided and carburized layers, respectively. The reciprocation sliding wear performances of the untreated, nitrided and carburized specimens were compared under both unlubricated (dry) and corrosive (in 0.5 M H_2SO_4 solution) conditions. The results show that under dry sliding conditions, both the nitrided layer and carburized layer can offer good wear resistance to 316L steel. The total material loss (TML) of the steel is reduced by more than two orders of magnitude by low temperature nitriding, while low temperature carburizing offers a reduction in TML by an order of magnitude. The better dry sliding wear performance of the nitrided layer is attributed to its much higher hardness as compared to the carburized layer. However, under corrosive-wear conditions in 0.5 M H_2SO_4 solution, the wear performance of the nitrided layer is significantly deteriorated, with TML 100% higher than that of the untreated 316L steel. On the other hand, the carburized layer can still offer good wear resistance in the corrosive environment, with a reduction in TML of 316L steel by 40%. This research has practical implication that low temperature nitriding is the most suitable for applications in dry and non-corrosive environments, while low temperature carburizing is more suitable for applications in H_2SO_4-containing corrosive environments.

1. Introduction

It has been established that low temperature nitriding (LTN) and low temperature carburizing (LTC) can improve the wear performance of austenitic stainless steels without compromising their excellent corrosion resistance (Ref 1-6). Due to the relatively low treatment temperatures employed during these processes, the formation of chromium nitrides and chromium carbides can be suppressed, such that a precipitation-free nitrided layer and a precipitation-free carburized layer can be formed, respectively. The LTN layer is composed of nitrogen expanded austenite (or nitrogen S-phase) and the LTC layer is composed of carbon expanded austenite (or carbon S-phase) (Ref 2-4, 7), both possessing a high hardness and good corrosion resistance. In general, LTC can be carried out at higher temperatures (below 500 °C) than LTN (below 450 °C), such that a thicker precipitation-free layer can be produced by LTC than by LTN, but the LTC layer is not as hard as the LTN layer (Ref 2-4). Various surface treatment techniques can be

used to conduct the low temperature processes, including plasma (Ref 1, 7-9), gaseous (Ref 10-13), liquid salt bath (Ref 14, 15) and fluidized bed (Ref 16) processes.

The wear performances of LTN and LTC austenitic stainless steels have been studied by many investigators during the past two decades (Ref 17-22). Most of the tribological tests have been conducted under dry unlubricated conditions (Ref 22, 23), and limited work has also been done in corrosive-wear conditions (Ref 24, 25). As confirmed by many investigators, the dry sliding wear resistance of austenitic stainless steels can be enhanced by one to two orders of magnitude by these two processes. The wear performance is also affected by the counter-body material (Ref 17, 26) and the test conditions (Ref 27). Under corrosive-wear conditions, the low temperature carburized layer performed well in NaCl and H_2SO_4 containing solutions (Ref 24), while the performance of the low temperature nitrided layer in a corrosive liquid solution was not as good as expected (Ref 25).

Due to the difference in layer thickness, hardness and electrochemistry between the LTN and LTC layers, it is expected that these two layers perform quite differently under both dry and corrosive-wear conditions. Although the wear performances of the LTN and LTC layers have been studied separately, very limited study has been conducted to compare the wear performance of these two layers under the same dry sliding and corrosive-wear conditions. Duart et.al. (Ref 23) studied the dry sliding friction and wear behavior of LTN, LTC and sequential LTC and LTN 316 L steel under conditions where the hardened layers were completely worn through. They found that there was a transition in frictional behavior when the hardened layers were worn through and the sequential process

Y. Sun and **R. Bailey**, School of Engineering and Sustainable Development, Faculty of Computing, Engineering and Media, De Montfort University, Leicester LE2 4TX, UK. Contact e-mail: ysun01@dmu.ac.uk.

offered the best wear resistance. However, the work (Ref 23) did not provide sufficient information regarding the inherent wear resistance of the LTN layer as compared to that of the LTC layer. In order to maximize the application potentials of these low temperature processes in different environmental conditions, it is necessary to conduct comparative studies on the wear performances of the LTN and LTC layers under the same conditions. In the present work, the reciprocation sliding wear performances of the untreated, nitrided and carburized specimens were compared under both unlubricated (dry) and corrosive (in 0.5 M H_2SO_4 solution) conditions. This paper presents the obtained results and discusses the wear mechanisms involved.

2. Materials and Methods

2.1 Material and Sample Preparation

316L austenitic stainless steel was used as the test substrate material in this work. The chemical composition of the substrate is as follows (in wt.%): 0.02%C, 18.61%Cr, 11.83%Ni, 2.37%Mo and balance Fe. A hot-rolled plate of 2 mm thickness was cut into specimens of 25mm × 20 mm sizes. The specimens were then manually ground using a series of SiC emery papers from grade P120 to grade P1200 to achieve a surface finish of 0.12 μm (R_a). Before plasma processing, the specimens were washed and finally cleaned in ethanol.

Low-temperature plasma nitriding and carburizing were carried out in the glow discharge of a plasma, following standard procedures described previously (Ref 8, 28). Plasma nitriding was carried out in a gas mixture of 80% N_2 and 20% H_2, at 415 °C for 15 h, while plasma carburizing was conducted in a gas mixture containing 98%H_2 and 2%CH_4, at 470 °C for 15 h. These treatment parameters were selected based on previous work (Ref 28) to ensure that a sufficiently thick precipitation-free nitrided layer and carburized layer were respectively produced. Different temperatures were used for nitriding and carburizing because the steel responded differently to these two low-temperature surface alloying treatments (Ref 2-4). The thickness and hardness of the two layers tested in this work are summarized in Table 1. Figure 1 shows the nitrogen and carbon concentration profiles measured across the respective layers by glow discharge spectrometry, together with microscopic images showing the layer morphology. The 7.5-μm thick nitrided layer produced at 415 °C is very hard with a surface hardness of about 1200 $HV_{0.05}$. The carburized layer is much thicker (28 μm) and possesses a lower surface hardness of about 870 $HV_{0.05}$. Both layers were resistant to the etchant used to reveal the microstructure (50 vol% HCl + 25 vol%

HNO_3 + 25 vol% H_2O), such that they appear "white" under optical microscope. X-ray diffraction could only detect nitrogen expanded austenite in the nitrided layer and carbon expanded austenite in the carburized layer. No nitrides and carbides were detected in the respective layers.

2.2 Dry and Corrosive Sliding Wear Tests

Dry sliding and corrosive sliding wear tests were conducted using a laboratory scale reciprocating tribometer. During the test, the flat specimen was sliding reciprocally against a stationary slider, which was an alumina (Al_2O_3) ceramic ball of 8-mm diameter with a surface finish of 0.05 μm (R_a) and a hardness of 1800 HV. The reciprocating frequency and stroke amplitude were 2 Hz and 9 mm, respectively. All the tests were done under a contact load of 10 N, which is a typical contact load employed in several reported work (Ref 22, 23, 26, 27). This resulted in a maximum contact pressure of 1250 MPa on the untreated specimen at the initial contact, based on the calculation using the Hertzian contact theory. Although the classic Hertzian contact theory could not be applied to the nitrided and carburized specimens due to their layered structure, the initial contact pressures of these specimens could be estimated numerically, which requires knowing the Young's modulus values of the nitrided and carburized layers. To the best knowledge of the authors, there have been no reported measurements on the Young's modulus values of low temperature nitrided and carburized layers. However, it is reasonable to assume that the initial contact pressures on the nitrided and carburized specimens were similar to that on the untreated
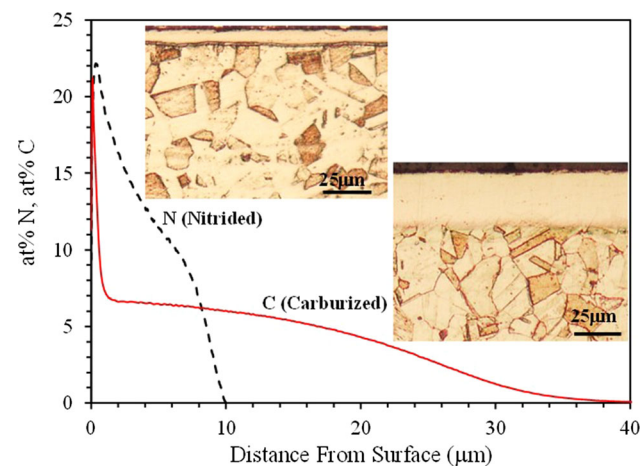
Fig. 1 Nitrogen and carbon concentration profiles and microscopic images of the nitrided and carburized specimens. The carburized layer was produced at 470 °C for 15 h and the nitrided layer was produced at 415 °C for 15 h

Table 1 Summary of nitrided and carburized layer thickness and hardness and sliding coefficient of friction

| Sample | Alloyed layer characteristics | | Coefficient of friction | |
	Thickness, μm	Surface hardness ($HV_{0.05}$)	Dry	0.5 M H_2SO_4
Untreated	0	210 ± 15	0.66 ± 0.044	0.40 ± 0.024
Carburized	28 ± 1	870 ± 35	0.70 ± 0.045	0.32 ± 0.021
Nitrided	7.5 ± 1	1200 ± 41	0.71 ± 0.041	0.33 ± 0.025

specimen because both the nitrided and carburized layers had an expanded austenite structure and thus should have a similar Young's modulus to that of the austenitic substrate. Furthermore, as wear progressed, the contact area was increased and thus the contact pressure would decrease, thus the effect of initial contact pressure would diminish. The sliding time was 7200 s for all tests, corresponding to a total sliding distance of 258.2 m. During each test, the frictional force was recorded continuously and the coefficient of friction was calculated by dividing the friction force by the contact load. All tests were repeated to check the consistence of results. All tests were conducted at room temperature (22 °C). Dry sliding tests were done in ambient environment with a humidity of 60%.

Corrosive-wear tests were conducted in 0.5 M H_2SO_4 aqueous solution made from analytical grade H_2SO_4 acid and double-distilled water. In order to ensure that corrosion only occurs to the test area of the specimen during corrosive-wear test, the specimen holder and the ball holder were made of an insulating material, nylon. The test specimen was masked with insulating lacquer to leave a test area of 15 mm × 8 mm exposing to the solution. Before the start of sliding, the specimen was rest in the solution for 900 s without contacting the Al_2O_3 ball. After sliding for 7200 s in the solution, the ball was removed from the contact and the specimen was rest in the solution for further 300 s. An ACM Gill AC potentiostat was used to measure the OCP of the specimen during the whole test period, using a saturated calomel electrode (SCE) as the reference electrode.

After the tests, the wear tracks were examined under optical and scanning electron microscopes. The Nikon optical microscope (Eclipse LV150N) had an extended-depth-of-focus function for capturing 3-dimensional images and surface profiling. The scanning electron microscope (Carl Zeiss EVO LS 15) was equipped with EDX facilities for elemental composition analysis. The cross-sectional profiles of the wear tracks were measured by a Taylor-Hobson stylus profilometer (Surtronic Intra Touch) to assess the actual depth and width of the tracks and the amount of material removal.

3. Results and Discussion

3.1 Dry Sliding Wear Performance

Figure 2(a) and (b) shows the surface profiles measured across the wear tracks on the test specimens. It can be seen that under the present dry sliding conditions, a deep and wide wear track was generated on the untreated specimen with a wear depth more than 70 μm. Severe plastic deformation in the contact area of the untreated specimen is evident as can been from the formation of two lips of more than 10 μm height at the edges (Fig. 2a). On the other hand, the wear track on the carburized specimen is much smaller, with a wear depth about 17 μm (Fig. 2b), which is smaller than the thickness of the carburized layer (28 μm). Thus, wear occurred within the carburized layer, which had better resistance to plastic deformation as evidenced by the much smaller height of the lips formed at the edges of the wear track. On the nitrided specimen, a very small wear track was generated, with a wear depth about 1.5 μm, which is much smaller than the nitrided layer thickness (7.5 μm). It is also evident that the nitrided layer resisted plastic
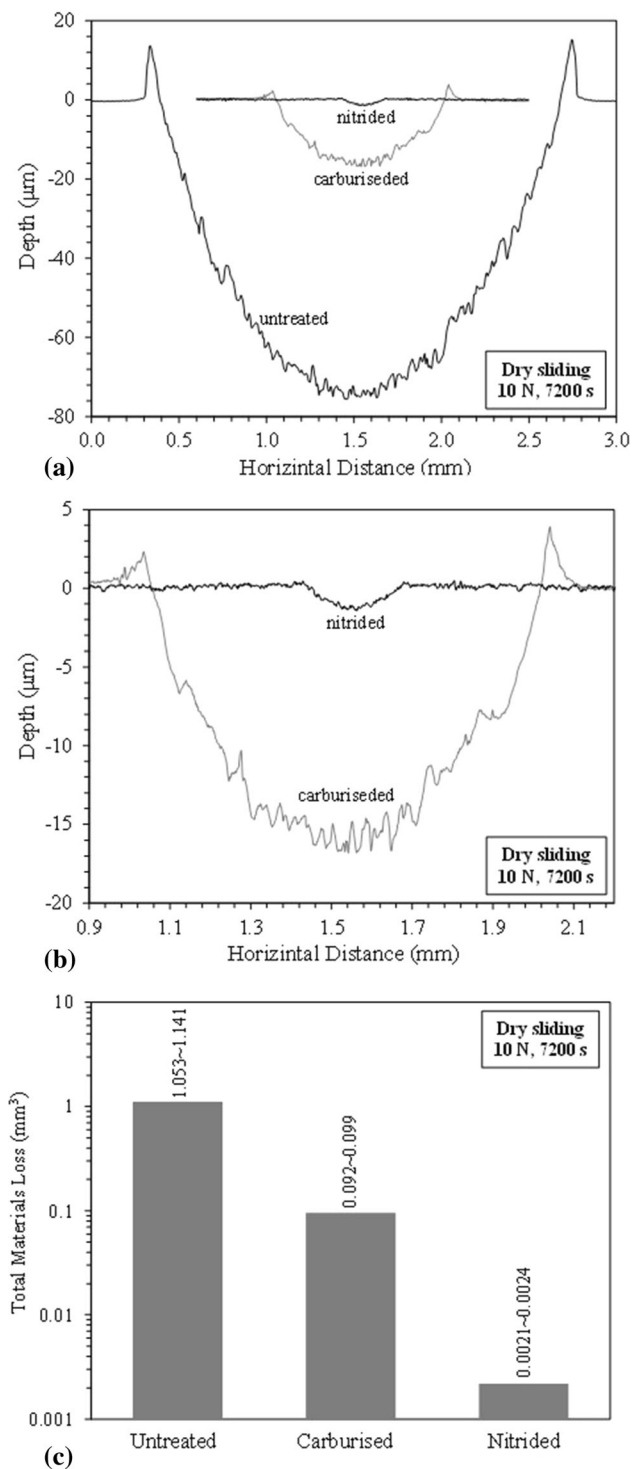
Fig. 2 Comparison of the cross-sectional profiles of the wear tracks (a and b) and total material loss from the wear tracks (c), resulted from dry sliding under 10 N load for 7200 s

deformation effectively, as no lips were formed at the edges of the wear track (Fig. 2b).

The total material loss (TML) from each wear track was estimated from the wear track profiles and the results are summarized in Fig. 2(c). Clearly, low temperature carburizing reduced the TML of 316L stainless steel by more than an order of magnitude, which agrees with the results reported by other

investigators (Ref 22, 23, 29, 30). Furthermore, low temperature nitriding offered even better dry sliding wear resistance: it reduced the TML of the steel by more than two orders of magnitude. Since the wear depth is smaller than the respective layer thickness (Fig. 2b), it is thus obvious that the nitrided layer possesses much better dry sliding wear resistance than the carburized layer under the present testing conditions.

The surface morphologies of the dry sliding wear tracks are shown in Fig. 3. In consistence with surface profile measurements shown in Fig. 2(a) and (b), the wear track on the untreated specimen (Fig. 3a) is wide and rough with many parallel abrasion marks. Under higher magnifications, there are clear signs of scoring, adhesion and delamination wear, see Fig. 3(d). Thus, the severe wear of the untreated specimen was the result of abrasive wear, adhesive wear and delamination wear, originating from the low surface hardness and the severe plastic deformation during the wear process. On the other hand, the wear track on the nitrided specimen is very narrow with a much smoother surface which has a combination of polished bright areas and some discolored areas (Fig. 3c), which are signs of micro-abrasion and oxidation, respectively. Indeed, detailed examination (Fig. 3e) revealed two distinct regions in the wear track: smooth regions with a polished appearance due to micro-abrasion and rough regions with the formation and removal of oxide products. EDX analysis detected more oxygen in the oxidized areas than in the polished areas. Obviously, the hard nitrided layer was effective in eliminating plastic deformation and adhesive wear, such that mild abrasive wear and oxidative wear were dominant, resulting in much reduced TML (Fig. 2c).

For the carburized specimen, the resultant dry sliding wear track (Fig. 3b) is much narrower than that on the untreated specimen (Fig. 3a), but is much wider and rougher than that on the nitrided specimen (Fig. 3c). The wear track on the carburized specimen is populated with many parallel abrasion marks, without obvious signs of adhesive wear and delamination wear. Although the carburized layer could not completely eliminate plastic deformation during the sliding contact (Fig. 2b), it was sufficient to prevent severe adhesion and delamination, such that abrasive wear became dominant.

In order to compare the wear mechanisms of the carburized and nitrided layers, the worn surfaces were further examined three dimensionally under higher magnifications, using the extended-depth-of-focus and surface profiling functions of the microscope, as shown in Fig. 4. Clearly, the carburized layer was worn by abrasion along the sliding directions which resulted in a rough worn surface, while the nitrided layer was worn by micro-polishing which resulted in a polished appearance. Both layers also suffered from oxidative wear due to the relatively high friction, which resulted in frictional heating and oxidation of the contact areas during sliding. The average values of coefficient of friction (COF) recorded during dry sliding are summarized in Tale 1. The nitrided and carburized layers showed slightly higher COF than the untreated specimen. All test specimens exhibited dry sliding COF ranging between 0.66 and 0.71. This agrees with the results of other investigators (Ref 26, 27) that the low temperature nitrided and carburized layers do not possess lower COF than the untreated steel under dry sliding conditions. The higher hardness of the nitrided and carburized layers can provide a larger resistance to
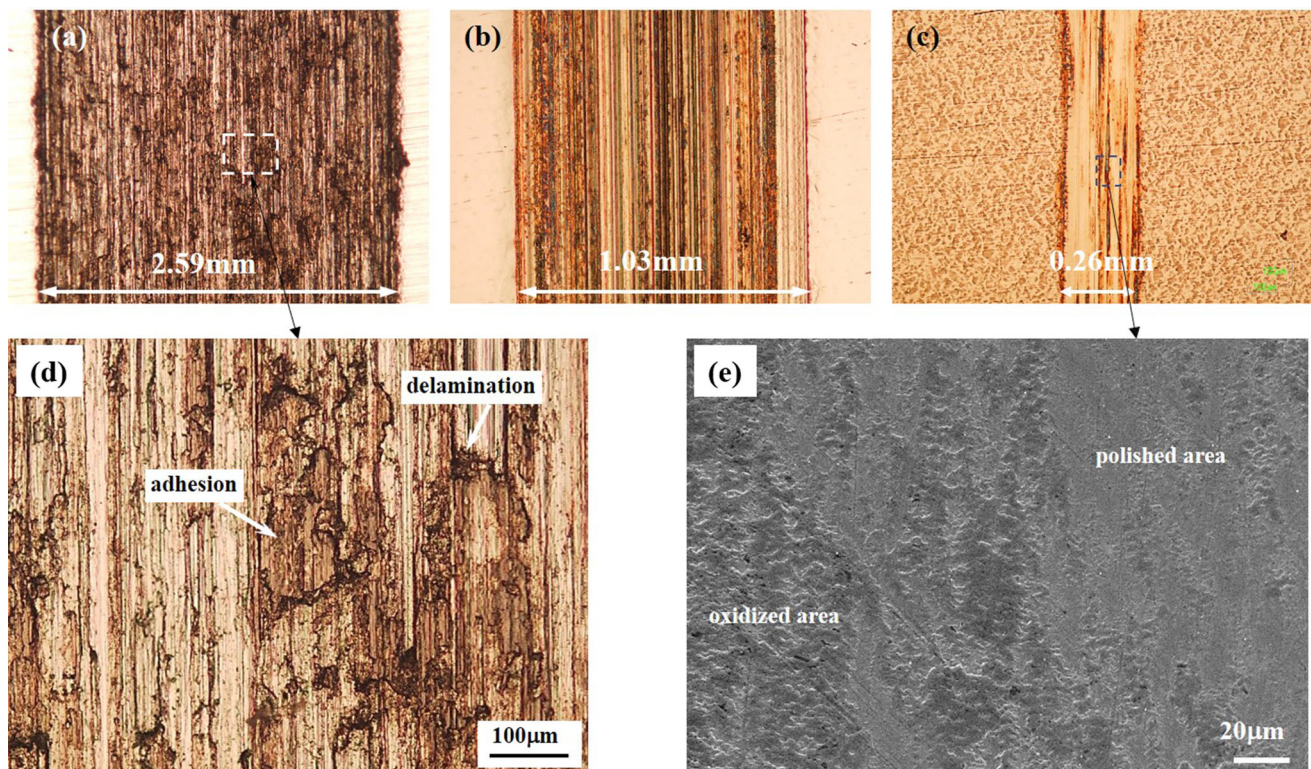
Fig. 3 Microscopic images showing the dry sliding wear tracks produced on the (a) untreated, (b) carburized, (c) nitrided specimens, (d) enlarged view of the worn surface of the untreated specimen and (e) SEM image of the worn surface of the nitrided specimen
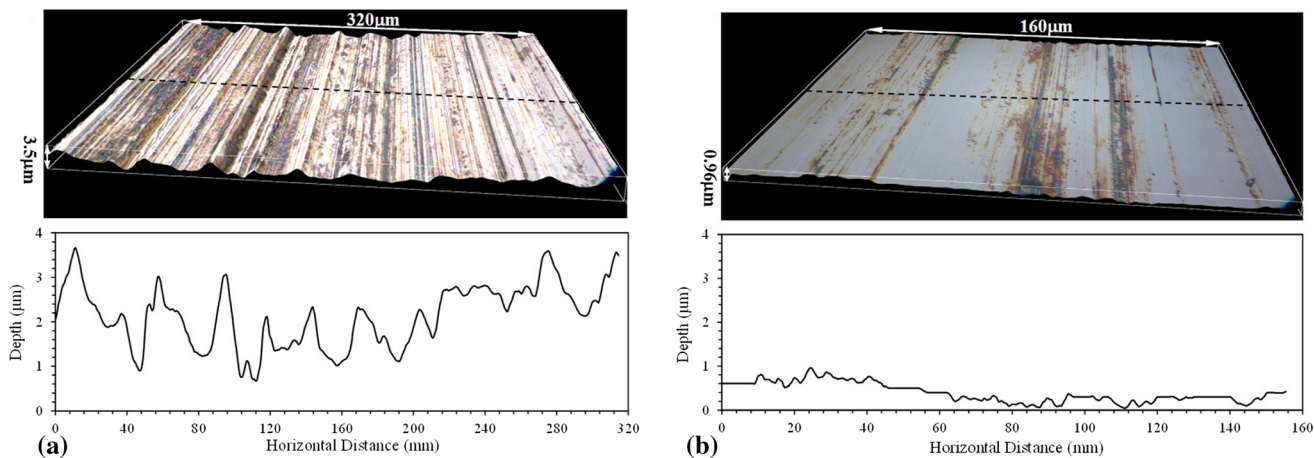
Fig. 4 3D microscopic images showing the worn surface and corresponding surface profile measured along the dashed line of the (a) carburized and (b) nitrided specimen, after dry sliding under 10 N for 7200 s
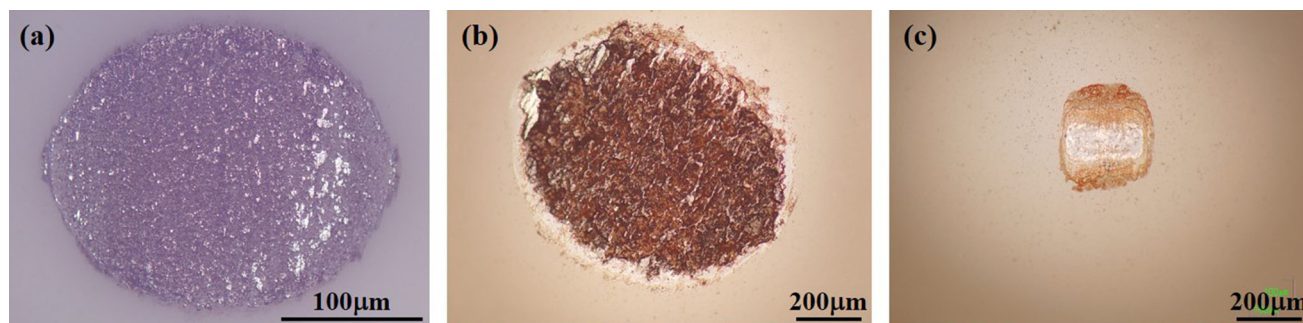
Fig. 5 Microscopic images showing the wear scars on the alumina balls after dry sliding with the (a) untreated, (b) carburized and (c) nitrided specimens under 10 N for 7200 s

shearing at the friction interface and thus may be responsible for their slightly higher COF, as compared to that of the untreated substrate.

Figure 5 shows the wear scars on the corresponding counter-bodies (Al_2O_3 balls) after dry sliding wear tests. Strong interaction between the specimen and the alumina ball occurred in the untreated specimen-Al_2O_3 ball couple, resulting in not only the observed severe wear of the specimen (Fig. 2c), but also a large amount of material loss from the Al_2O_3 ball (Fig. 5a). The interaction between the specimen and the Al_2O_3 ball was weakened by low temperature carburizing (Fig. 5b), which resulted in much reduced materials loss from both the specimen and the ball. Low temperature nitriding was the most effective in minimizing the interaction between the specimen and the Al_2O_3 ball (Fig. 5c), and thus was the most effective in reducing material loss from the sliding couple.
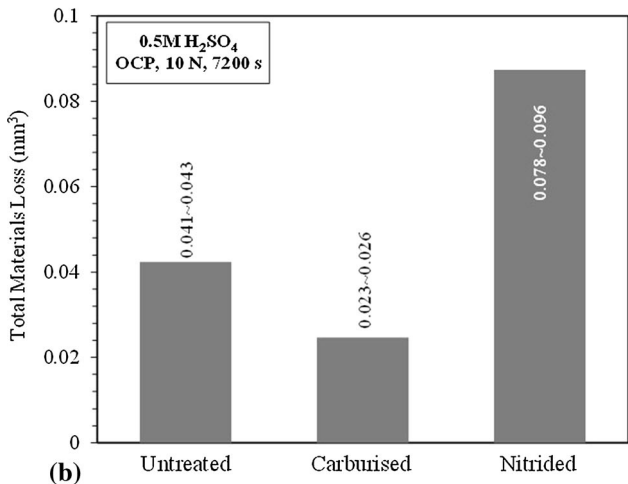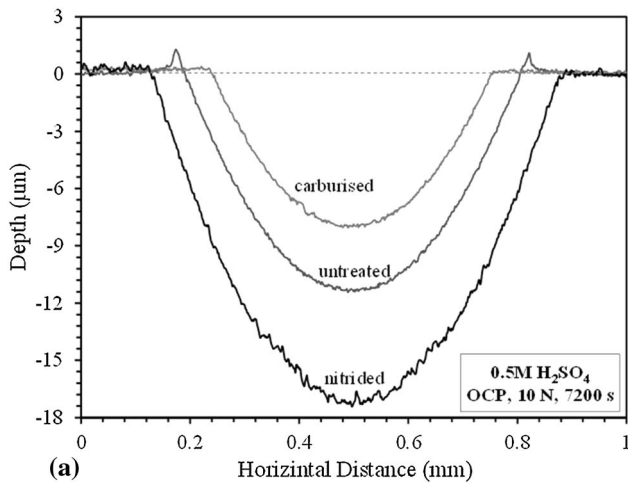
The results presented above demonstrate that although the nitrided layer was thinner than the carburized layer, it possessed much better dry sliding wear resistance. This can be attributed to the higher hardness of the nitrided layer (1200 HV), as compared to that of the carburized layer (870 HV), and thus the better ability of the nitrided layer to resist plastic deformation, adhesive wear, delamination wear and abrasive wear.

Under the present testing conditions, according to the Hertzian theory, the initial contact between the alumina ball and the flat specimen resulted in an initial contact area of radius 45 μm, and the maximum shear stress occurred at 22 μm below the surface, which was smaller than the carburized layer

thickness but larger than the nitrided layer thickness. Thus, the thicker carburized layer was expected to have better resistance to subsurface deformation than the thinner nitrided layer, at least at the initial stage of contact. However, as wear progressed, the contact area was increased and the high friction during sliding would move the maximum shear stress toward the surface. Thus, the properties of the surface layer played an important role in affecting dry sliding wear. This explains why the thinner but harder nitrided layer exhibited better dry wear resistance than the carburized layer.

3.2 Corrosive-Wear Performance

The results presented in the previous section demonstrate that the nitrided layer possesses the best wear resistance under dry sliding conditions. However, under corrosive sliding conditions in 0.5 M H_2SO_4 solution, the wear performance of the nitrided layer was seriously deteriorated, as shown in Fig. 6, which compares the cross-sectional profiles and TML of the wear tracks after sliding in 0.5 M H_2SO_4 solution at open circuit potential. The wear track on the nitrided specimen is wide and deep with a wear depth of 17 μm, which is much larger than that produced after dry sliding (1.5 μm). Since the thickness of the nitrided layer is about 7.5 μm, it is obvious that the nitrided layer was worn through during sliding in the corrosive solution. As a result, the TML from corrosive-wear (Fig. 6b) was nearly 40 time larger that from dry sliding (Fig. 2c). Clearly, wear of the nitrided specimen was acceler-

Fig. 7 Open circuit potential recorded for the test specimens during corrosive-wear in 0.5 M H$_2$SO$_4$ at open circuit potential under 10 N load
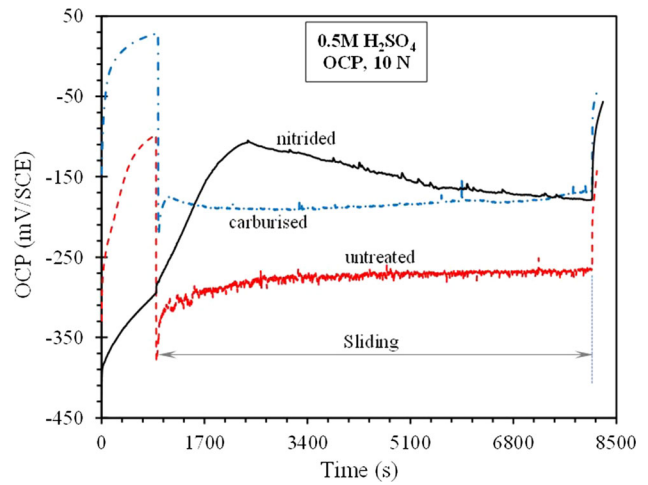
Fig. 6 Comparison of the cross-sectional profiles of the wear tracks (a) and total material loss from the wear tracks (b), resulted from corrosive-wear in 0.5 M H$_2$SO$_4$ at open circuit potential under 10 N load for 7200 s

ated by corrosion, a common phenomenon observed in corrosive-wear systems (Ref 31-34).

On the other hand, the untreated and carburized specimens showed different corrosive-wear behavior from the nitrided specimen. As shown in Fig. 6 and compared with Fig. 2, the wear depth and TML of these two specimens are smaller under corrosive-wear conditions than under dry sliding conditions. The TMLs of the untreated and carburized specimens resulting from sliding in the corrosive solution were, respectively, 96 and 74% smaller than those resulting from dry sliding. When comparing the corrosive-wear behavior of the three specimens, it is clear from Fig. 6 that the carburized layer was effective in improving the corrosive-wear resistance of 316L steel by 40%, while the corrosive-wear resistance of the nitrided layer was inferior to that of the untreated steel.

The reduction in TML during corrosive sliding of the untreated and carburized specimens, as compared to dry sliding, can be explained by the lubricating effect of the solution. Under the present testing conditions, the corrosive solution could produce boundary lubrication to all the sliding contact pairs (Ref 35), which could reduce the mechanical interactions between the two contact surfaces and result in

reduced mechanical wear. This explains why the COF of all the sliding pairs was reduced when tested in the corrosive solution (Table 1). However, the corrosive solution could also lead to corrosion and corrosion-accelerated wear (Ref 33, 34, 36). The response of the specimens to corrosion and corrosion-accelerated wear determines the different corrosive-wear behavior of the specimens, as discussed further below.

Figure 7 shows the open circuit potentials (OCP) recorded during the tests. Each OCP vs time curve can be divided into three regions: (1) the first 900 s region when the specimen was rest in the solution without sliding contact with the Al$_2$O$_3$ ball; (2) the sliding region between 900 and 8100 s when the specimen was sliding against the Al$_2$O$_3$ ball, resulting in material removal; and (3) the final region when sliding was completed and the specimen was rest in the solution for further 300 s.

From Fig. 7, it can be seen that, in the first region of 900 s without sliding, the OCP of all specimens increased with resting time in the solution, which was due to the gradual build-up of a passive film on the surface (Ref 24, 33, 35). The carburized specimen had the highest OCP in this region, indicating that the carburized surface was in the most passive state and thus had the best corrosion resistance. On the other hand, the nitrided specimen had the lowest OCP, indicating that it was in a more active state and had the worst corrosion resistance.

In the sliding region, the start of sliding led to an immediate drop in OCP of the untreated and carburized specimens. This is typical of passive metals during corrosive-wear, sliding can damage or remove the passive film, leading to the depassivation of the sliding track and thus a drop in OCP (Ref 24, 36). During the sliding period, the OCP of the untreated and carburized specimens remained relatively stable, resulting from the repeated depassivation and repassivation of the wear track during the reciprocating sliding cycles (Ref 33). It is also noted that during the sliding period, the OCP of the carburized specimen was always higher than that of the untreated specimen, thus the wear track on the carburized layer was in a less active state than that on the untreated specimen.

However, the response of the nitrided specimen to OCP evolution during sliding was different from that observed for

passive systems. Instead, the OCP of the nitrided specimen increased during the first 1600 s sliding, until a maximum was reached, then it decreased with further sliding. Considering the fact that the nitrided layer was worn through during sliding in the corrosive solution (Fig. 6a), it is reasonable to assume that the increase in OCP during the first 1600 s sliding was due to sliding within the nitrided layer, while the decrease in OCP during the second stage was due to the wearing-through of the nitrided layer and the gradual exposal of the untreated substrate to the solution, thus the OCP response gradually approached that of the untreated specimen. Such a peculiar behavior could be explained by the variation of passivity of the nitrided layer with depth from the surface. Although only a single expanded austenite phase was detected by XRD in the nitrided layer, it is likely that small amounts of chromium nitrides were formed at grain boundaries in the near surface region of the layer where the nitrogen content was the highest (Fig. 1). Thus, grain boundaries at the surface were preferential sites for corrosion attack, enhancing the activity of the nitrided surface (Ref 2, 28). With increasing depth from the surface, the bulk of the nitrided layer should become less active because the layer was free of nitride precipitation. Therefore, during the early stage of sliding, the active surface region was gradually removed and the bulk of the nitrided layer was exposed, leading to the gradual increase in OCP. After the nitrided layer was worn through, the wear track was now characteristic of a passive metal and started to experience a drop in OCP during further sliding.

Figure 8 shows the microscopic images of the wear tracks on the specimens and the corresponding wear scars on the counter-body Al_2O_3 balls after sliding tests in the corrosive solution. Unlike the dry sliding situation (Fig. 5a) where significant material loss from the ball was evident for the untreated specimen-Al_2O_3 ball pair, sliding in the corrosive solution resulted in much reduced material loss from the ball (Fig. 8a). Correspondingly, the wear track on the untreated specimen was much narrower with some parallel scratch marks. The principal wear mechanisms of the untreated specimen in the corrosive solution were abrasive wear and chemical wear due to the repeated formation and removal of the passive film (Ref 24, 33, 36). In the case of the carburized specimen-Al_2O_3 ball pair, wear of the ball was hardly noticeable, and the wear track on the carburized layer was very smooth with a shiny polished appearance (Fig. 8b). Thus, chemical wear in the form of repeated formation and removal of the passive film was mainly responsible for the material loss from the wear track on the carburized layer, resulting in a polished surface, which is similar to electropolishing (Ref 37). On the other hand, on the nitrided specimen, a much wider and rougher wear track was produced in the corrosive solution, and the corresponding wear scar on the ball was larger with some scratches (Fig. 8). The nitrided layer was worn through during sliding, evidenced from the two edges of the wear track which reveal the nitrided layer (Fig. 8c). This is more clearly seen in an enlarged view shown in Fig. 9, which reveals the substrate and the nitrided layer in the wear track and the surface (outside the wear track) exposed to the corrosive solution. Clearly, the nitrided layer was worn through such that the substrate was exposed in the wear track. Interestingly, the surface outside the wear track has a dark and corroded appearance. The grain boundaries in the near surface region of the nitrided layer were also attacked by the solution. This agrees with the variation of OCP values of the nitrided layer with sliding time, shown in Fig. 7, and confirms that the near surface region of the nitrided layer was more active than the interior of the nitrided layer.
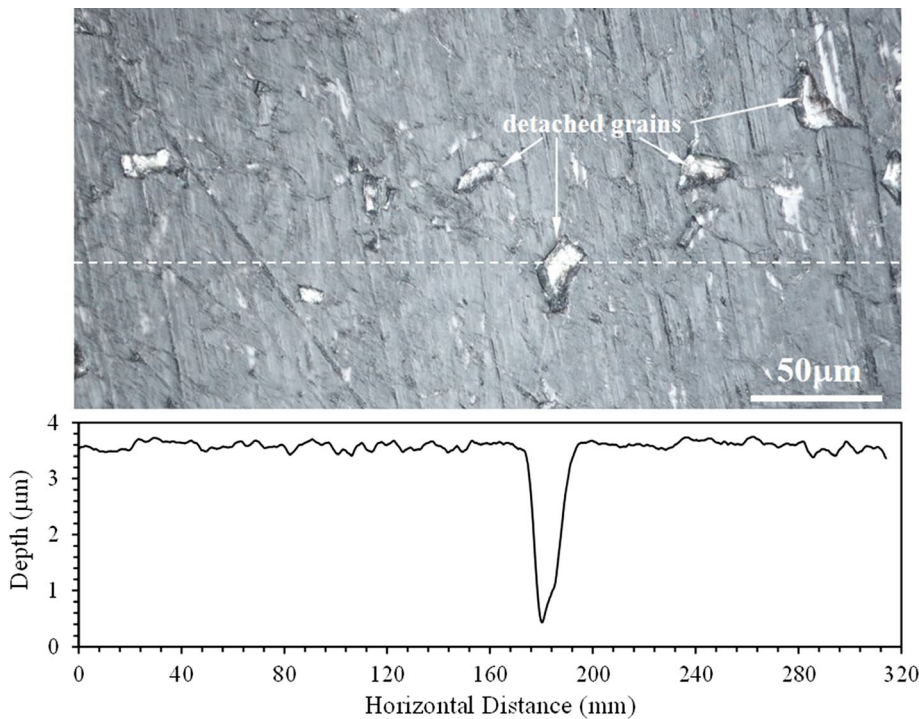
Figure 10 is a microscopic image showing the nitrided surface outside the wear track, which was exposed to the corrosive solution during the test period of 8400 s. It can be seen that the surface was severely corroded with a dark film formation. Some grains in the nitrided layer were detached from the surface as a result of corrosion alone, as confirmed by the surface profile across one of the detached areas. This
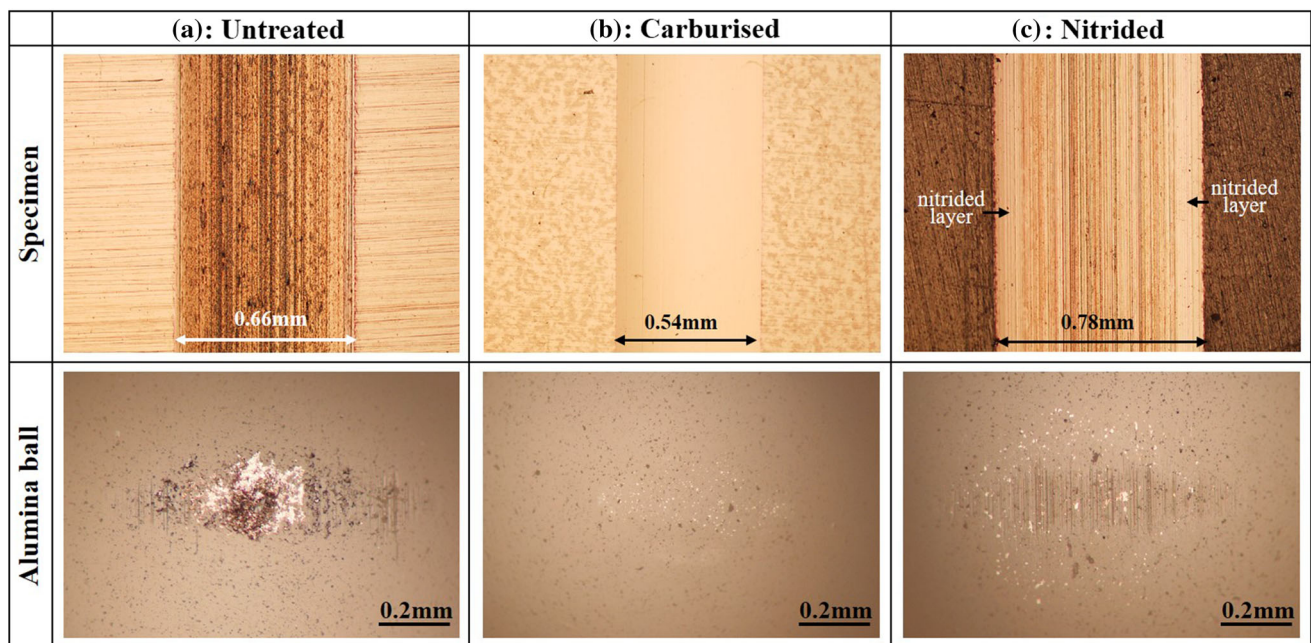
Fig. 8 Microscopic images showing the corrosive-wear tracks on the specimens and the corresponding wear scars on the alumina balls, resulted from sliding in 0.5 M H_2SO_4 at open circuit potential under 10 N load for 7200 s
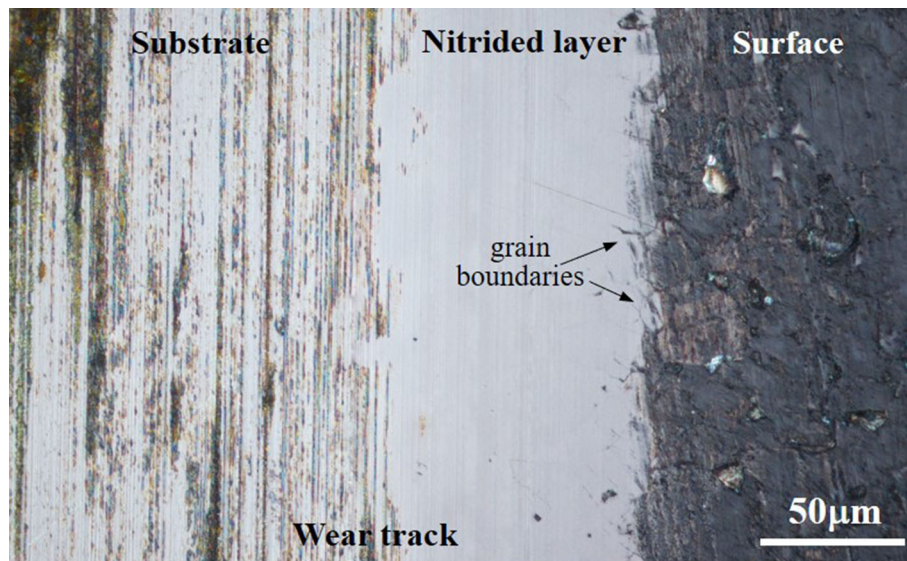
Fig. 9 Microscopic image showing an enlarged view of the edge of the corrosive-wear track on the nitrided specimen shown in Fig. 8(c)

Fig. 10 Microscopic image showing the nitrided surface exposed to the 0.5 M H_2SO_4 solution outside the wear track area. The surface profile was measured along the dashed line, showing the detachment of a grain from the surface

confirms that the nitrided surface suffered from active metal dissolution in the corrosive solution.

Total material loss (T) during corrosive-wear results from mechanical wear (W_0), corrosion (C_0) and the synergism between wear and corrosion (S). The synergism between wear and corrosion can be calculated as follows (Ref 31, 38):

$$S = T - W_0 - C_0 \qquad \text{(Eq 1)}$$

In Eq (1), T can be measured after corrosive-wear tests, as shown in Fig. 6 and listed in the second column of Table 2. In order to calculate the synergism, S, additional tests are

necessary to find W_0 and C_0. To find W_0, further sliding tests were conducted in the solution at a cathodic potential of − 900 mV(SCE), where material loss during sliding was predominantly due to mechanical wear because corrosion at cathodic potentials was insignificant. Such an approach was initially used by Watson et al. (Ref 31). The total material loss results (W_0) under such a cathodic protection condition are listed in the third column of Table 2. Furthermore, to find C_0, potentiodynamic tests were conducted in the test solution at a scan rate of 1 mV/s from − 300 mV (vs rest potential) to 1000 mV (vs rest potential). Figure 11 shows the measured polarization curves for the three test specimens. It can be seen

Table 2 Summary of measured material losses due to mechanical wear and corrosion and calculated synergism

Sample	T, mm³ (at OCP)	W₀, mm³ at − 900 mV(SCE))	C₀, mm³ (at OCP)	S, mm³ (calculated, Eq (1))	S/T × 100 (% synergism)
Untreated	4.24×10^{-2}	2.73×10^{-2}	5.80×10^{-4}	1.45×10^{-2}	34
Carburized	2.47×10^{-2}	1.68×10^{-2}	2.49×10^{-4}	7.65×10^{-3}	31
Nitrided	8.73×10^{-2}	4.61×10^{-3}	9.49×10^{-3}	7.32×10^{-2}	84
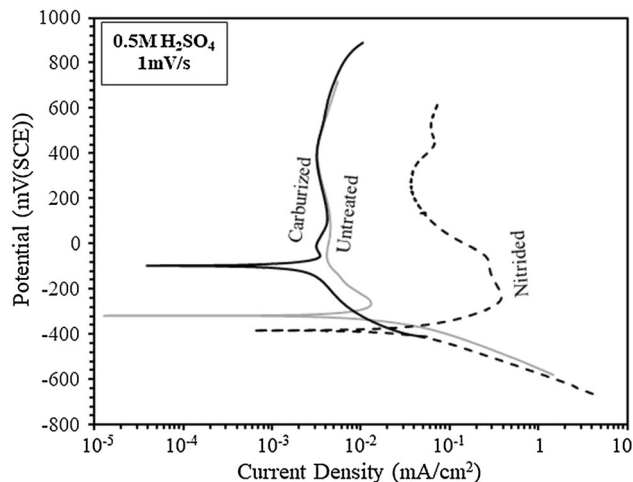
Fig. 11 Potentiodynamic polarization curves measured in 0.5 M H_2SO_4 solution for the test specimens

that all test specimens showed an active to passive transition in the anodic region. The untreated and carburized specimens showed much lower passivation current densities and better passivity than the nitrided specimen, confirming that the nitrided surface suffered from active metal dissolution, as discussed above. The Tafel method was used to estimate the corrosion current density and then the Faraday's law was used to calculate C_0 in volume, following standard procedures (Ref 31, 36). The fourth column of Table 2 lists the C_0 results at the rest potential. Finally, the synergism between wear and corrosion for each specimen was calculated using Eq (1) and the results are listed in the fifth column of Table 2.

From Table 2, it can be seen that for each specimen, the sum of W_0 and C_0 is smaller than the measured TML (T), confirming that there was wear-corrosion synergism which was responsible for the excessive amount of material loss during corrosive-wear at OCP. As expected, nitriding and carburizing effectively reduced mechanical wear (W_0), due to the high hardness of the expanded austenite layers. The contribution of pure corrosion to TML is insignificant in the untreated and carburized specimens ($< 1.5\%$) due to their passivity in the solution. However, pure corrosion had a noticeable contribution (11%) in the nitrided specimen, further confirming that the nitrided layer suffered from active metal dissolution (Fig. 11). Furthermore, the synergistic effect was the most significant in the nitrided specimen (84%) and the least significant in the carburized specimen (31%). It was the combined effect of the active metal dissolution and the sliding mechanical action that led to the significant synergistic effect and the observed much deteriorated corrosive-wear performance of the nitrided layer in the 0.5 M H_2SO_4 solution. On the other hand, the carburized layer had the ability to resist mechanical wear and the passivity to resist corrosion, and thus experienced a smaller synergistic effect between wear and corrosion.

It is expected that the corrosive-wear performances of the nitrided and carburized layers depend on the corrosive environmental conditions. Only one particular condition was studied in this work. Further research work is necessary to identify the application potentials of these two layers in different corrosive conditions.

4. Conclusions

(1) Both low-temperature plasma nitriding and carburizing are effective in improving the dry sliding wear resistance of 316 L austenitic stainless steel by one to two orders of magnitude, respectively.

(2) The thinner nitrided layer is more effective than the thicker carburized layer in improving the dry sliding wear resistance. This is due to the higher hardness of the nitrided layer which provides more resistance to plastic deformation, adhesive wear, delamination wear and abrasive wear.

(3) Under corrosive-wear conditions in 0.5 M H_2SO_4 solution, low temperature nitriding deteriorates the wear performance of 316L steel. The nitrided layer suffers from a large amount of material loss due to the combined effects of active metal dissolution and mechanical sliding actions.

(4) Low temperature carburizing is still effective in improving the wear performance of 316L steel under corrosive-wear conditions in 0.5 M H_2SO_4 solution. The carburized layer reduces the TML of the steel by 40%. This is due to its high hardness to resist mechanical wear and its passivity in the corrosive solution to resist chemical wear.

(5) This research suggests that low temperature nitriding is the most suitable for applications in dry and non-corrosive environments, while low temperature carburizing is more suitable for applications in H_2SO_4-containing corrosive environments.

References:

1. Z.L. Zhang and T. Bell, Structure and Corrosion Resistance of Plasma Nitrided Stainless Steel, *Surf. Eng.*, 1985, **1**, p 131–136

2. H. Dong, S-phase Surface Engineering of Fe-Cr, Co-Cr and Ni-Cr Alloys, *Int. Mater. Rev.*, 2010, **55**, p 65–98

3. F. Borgioli, From Austenitic Stainless Steel to Expanded Austenite S-phase: Formation, Characteristics and Properties of an Elusive Metastable Phase, *Metals*, 2020, **10**, p 1–46

4. Y. Sun, Production of Nitrogen and Carbon S Phases in Austenitic Stainless Steels by Hybrid Plasma Surface Alloying, *Surf. Eng.*, 2010, **26**, p 114–122

5. Y. Li, Y. He, W. Wang, J. Mao, L. Zhang, Y. Zhu, and Q. Ye, Plasma Nitriding of AISI 304 Stainless Steel in Cathodic and Floating Electric Potential: Influence on Morphology, Chemical Characteristics and Tribological Behaviour, *J. Mater Eng. Perform.*, 2018, **27**, p 948–960

6. Y.E. Nunez de la Rosa, O.P. Calabokis, P.C. Borges, and V.B. Ballesteros, Effect of low Temperature Plasma Nitriding on corRosion and Surface Properties of Duplex Stainless Steel UNS32205, *J. Mater Eng. Perform.*, 2020, **29**, p 2612–2622

7. X. Tao, X. Liu, A. Matthews, and A. Leyland, The Influence of Stacking Fault Energy on Plasticity Mechanisms in Triode-Plasma Nitrided AUSTENITIC Stainless Steels: Implications for the Structure and Stability of Nitrogen-Expanded Austenite, *Act Mater.*, 2019, **164**, p 60–75

8. Y. Sun, X.Y. Li, and T. Bell, Low Temperature Plasma Carburising of Austenitic Stainless Steels for Improved Wear and Corrosion Resistance, *Surf. Eng.*, 1999, **15**, p 49–54

9. G.Y. Li and M.K. Lei, Microstructure and Properties of Plasma Source Nitrided AISI316 Austenitic Stainless Steel, *J. Mater Eng. Perform.*, 2017, **26**, p 418–423

10. M. Gillham, R. van der Jagt, and B. Kolster, New Case Hardening Process for Austenitic Stainless Steels, *Mater. World*, 1996, **12**, p 460–462

11. T. Christiansen and M.A.J. Somers, Low Temperature Gaseous Nitriding and Carburising of Stainless Steel, *Surf. Eng.*, 2005, **21**, p 445–455

12. T. Christiansen and M.A.J. Somers, On the Crystallographic Structure of S-Phase, *Scr. Mater.*, 2004, **50**, p 35–37

13. F. Ernst, D. Li, H. Kahn, G.M. Michal, and A.H. Heuer, The Carbide M_7C_3 in Low-Temperature-Carburized Austenitic Stainless Steel, *Acta Mater.*, 2011, **59**, p 2268–2276

14. Y. Lin, J. Wang, D. Zeng, R. Huang, and H. Fan, Advance Complex Liquid Nitriding of Stainless Steel AISI 321 Surface at 430 °C, *J. Mater. Eng. Perform.*, 2013, **22**, p 2567–2573

15. G. Prakash and S.K. Nath, Studies on Enhancement of Silt EROSION Resistance of 13/4 Martensitic Stainless Steel by Low Tow-Temperature Salt Bath Nitriding, *J. Mater. Eng. Perform.*, 2018, **27**, p 3206–3216

16. E. Haruman, Y. Sun, A. Triwiyanto, Y.H.P. Manurung, and E.Y. Adesta, An Investigation on Low-Temperature Thermochemical Treatments of Austenitic Stainless Steel in Fluidized Bed Furnace, *J. Mater. Eng. Perform.*, 2012, **21**, p 388–394

17. J. Buhagiar, A. Jung, D. Gouriou, B. Mallia, and H. Dong, S-Phase Against S-Phase Tribopairs for Biomedical Applications, *Wear*, 2013, **301**, p 280–289

18. Q. Luo, O. Oluwafemi, M. Kitchen, and S. Yang, Tribological Properties and Wear Mechanisms of DC Pulse Plasma Nitrided Austenitic Stainless Steel in Dry Reciprocating Sliding Tests, *Wear*, 2017, **376–377**, p 1640–1651

19. F.A.P. Fernandes, S.C. Heck, R.G. Pereira, C.A. Picon, P.A.P. Nascente, and L.C. Casteletti, Ion Nitriding of a Superaustenitic Stainless Steel: Wear and Corrosion Characterization, *Surf. Coat. Tech.*, 2010, **204**, p 3087–3090

20. K. Kovaci and Y. Secer, Improved Tribological Performance of AISI 316L Stainless Steel by a Combined Surface Treatment: Surface Texturing by Selective Laser Melting and Plasma Nitriding, *Surf. Coat. Tech.*, 2020, **400**, p126178

21. L. Ceschini, C. Chiavari, E. Lanzoni, and C. Martuni, Low Temperature Carburised AISI 316L Austenitic Stainless Steel: Wear and Corrosion Behaviour, *Mater. Des.*, 2012, **38**, p 154–160

22. B. Rayner, X.Y. Li, and H. Dong, Preliminary Study on Plasma Surface Modification of Medical Grade 316LVM and High Nitrogen Austenitic Stainless Steels, *Surf. Eng.*, 2006, **22**, p 103–108

23. M.C.S. Duarte, C. Godoy, and J.C.A. Wilson, Analysis of Sliding Wear Tests of Plasma Processed AISI 316L Steel, *Surf. Coat. Tech.*, 2014, **260**, p 316–325

24. Y. Sun, Tribocorrosion Behaviour of Low Temperature Plasma Carburized Stainless Steel, *Surf. Coat. Tech.*, 2013, **228**, p S342–S348

25. J. Baranowska, S.E. Franklin, and A. Kochmanska, Wear Behaviour of Low-temperature gas Nitrided Austenitic Stainless Steel in Corrosive Liquid Environment, *Wear*, 2007, **263**, p 669–673

26. L. Ceschini, C. Chiavari, A. Marconi, and C. Martini, Influence of the Countermaterial on the Dry Sliding Friction and Wear Behaviour of Low Temperature Carburized AISI316L Steel, *Trib. Int.*, 2013, **67**, p 36–43

27. F. Rotundo, L. Ceschini, C. Martini, R. Montanari, and A. Varone, High Temperature Tribological Behaviour and Microstructural Modifications of the Low-Temperature Carburized AISI 316L Austenitic Stainless Steel, *Surf. Coat. Tech.*, 2014, **258**, p 772–781

28. T. Bell and Y. Sun, Low Temperature Plasma Nitriding and Carburising of Austenitic Stainless Steels, *Heat Treat. Met.*, 2002, **29**(3), p 57–64

29. S. Corujeira Gallo, X. Li, and H. Dong, Dry Sliding Wear of Active Screen Plasma Carburised Austenitic Stainless Steel, *Trib. Let.*, 2012, **45**(1), p 153–160

30. M.A. Barcelos, M.V. Barcelos, J. de Sousa, A. Filho, A.R. Franco, and E.A. Vieira, Wear Resistance of AISI 304 Stainless Steel Submitted to Low Temperature Plasma Carburizing, *REM – Int. Eng. J.*, 2017, **70**(3), p 293–298. https://doi.org/10.1590/0370-44672016700094

31. S.W. Watson, F.J. Friedersdorf, B.W. Madsen, and S.D. Gramer, Methods of Measuring Wear-Corrosion Synergism, *Wear*, 1995, **181–183**, p 476–484

32. P.A. Dearnley and G. Aldrich-Smith, Corrosion-Wear Mechanisms of Hard Coated Austenitic 316L Stainless Steel, *Wear*, 2004, **256**, p 491–499

33. P. Ponthiaux, F. Wenger, D. Drees, and J.P. Celis, Electrochemical Techniques for Studying Tribocorrosion Processes, *Wear*, 2004, **256**, p 459–468

34. A.I. Munoz, N. Espallargas,, and S. Mischler Eds., *Tribocorrosion*, Springer, Berlin, 2020

35. S. Cao and S. Mischler, A Lubricated Tribocorrosion Model Incorporating Surface Roughness, *Biotribocorrosion*, 2021, **26**, 100181

36. Y. Sun and Vipul Rana, Tribocorrosion Behaviour of AISI 304 Stainless Steel in 0.5M NaCl Solution, *Mater. Chem. Phys.*, 2011, **129**(1–2), p 138–147. https://doi.org/10.1016/j.matchemphys.2011.03.063

37. S.-J. Lee, Y.-M. Lee, and Du. Ming-Feng, The Polishing Mechanism of Electrochemical Mechanical Polishing Technology, *J. Mater. Proc. Tech.*, 2003, **140**, p 280–286

38. Y. Nunez, M. Mafra, and R.E. Marales, Pautlo Cesar Borges, Giuseppe Pintaude, The Effect of Plasma Nitriding on the Synergism Between Wear and Corrosion of SAF 2205 Duplex Stainless Steel, *Ind. Lubr. Tribol.*, 2020, **72**(9), p 1117–1122